Guided Growth of Horizontal ZnO Nanowires with Controlled Orientations on Flat and Faceted Sapphire Surfaces

David Tsivion,[†] Mark Schvartzman,[†] Ronit Popovitz-Biro,[‡] and Ernesto Joselevich[†,*]

[†]Department of Materials and Interfaces and [‡]Chemical Research Support, Weizmann Institute of Science, Rehovot 76100, Israel

ABSTRACT

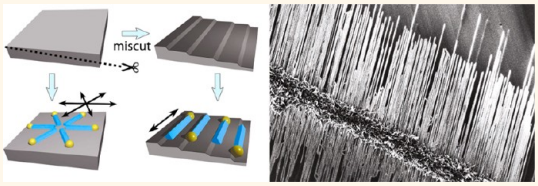

The large-scale integration of nanowires into practical devices is hindered by the limited ability to controllably assemble these nanoscale objects on surfaces. Following our first report on the guided growth of millimeter-long horizontal nanowires with controlled orientations, here we demonstrate the generality of the guided growth approach by extending it from GaN nanowires to ZnO nanowires. We describe the guided growth of horizontally aligned ZnO nanowires with controlled crystallographic orientations on eight different planes of sapphire, including both flat and faceted surfaces. The growth directions, crystallographic orientation, and faceting of the nanowires are constant for each surface plane and are determined by their epitaxial relation with the substrate, as well as by a graphoepitaxial effect that guides their growth along surface steps and grooves. These horizontal ZnO nanowires exhibit optical and electronic properties comparable to those of vertically grown nanowires, indicating a low concentration of defects. While the guided growth of ZnO nanowires described here resembles the guided growth of GaN nanowires in its general aspects, it also displays notable differences and qualitatively new phenomena, such as the controlled growth of nanowires with vicinal orientations, longitudinal grain boundaries, and thickness-dependent orientations. This article proves the generality of the guided growth phenomenon, which enables us to create highly controlled nanowire structures and arrays with potential applications not available by other means.

KEYWORDS: nanowires · zinc oxide · epitaxy · self-assembly · nanostructures · one-dimensional · bottom-up

During the past decade, semiconducting nanowires grown by the vapor–liquid–solid (VLS) method have been used as the building blocks of a plethora of nanodevices, promising a paradigm shift from a top-down to a bottom-up approach.[1] Notable examples include field-effect transistors,[2,3] lasers,[4,5] light-emitting diodes,[6,7] photovoltaic cells,[8–10] chemical and biological sensors,[11–13] and piezoelectric nanogenerators.[14] Many of these devices were demonstrated using serial and expensive fabrication methods such as electron-beam lithography, where each device was built around a randomly deposited nanowire with the desirable characteristics. In order to advance from proof-of-concept to practical devices, one must control the locations and orientation of a large assembly of nanowires. Several methods have been devised to control the orientation of nanowires on surfaces, such as using liquid flows,[15,16] electric fields,[17,18] Langmuir–Blodgett compression,[19–22] and mechanical shear.[23,24] Most of these methods involve harvesting the nanowires, suspending them in solution, and manipulating them in order to achieve the desired alignment. These processes usually damage the delicate nanowires, limiting the length to no more than a few tens of micrometers, and the alignment is not perfect due to thermal and dynamic fluctuations. Another inherent limitation of these postgrowth methods is the irreversible scrambling of the nanowire directionalities, which could be critical for the operation of devices based on polar nanowires,[25] nanowire heterojunctions with modulated doping,[26] or nanowires with axially modulated composition.[6]

An alternative to postgrowth assembly methods, which could overcome these limitations, is the "guided growth" approach, where the nanowires grow horizontally on the substrate and are aligned during the synthesis (Figure 1A, right). A similar approach has been extensively applied to carbon nanotubes.[27–29] However, for inorganic nanowires, horizontal growth has been reported using a limited number of materials and substrates, including ZnO nanowires on A-plane sapphire[30] and on

* Address correspondence to ernesto.joselevich@weizmann.ac.il.

Received for review May 10, 2012 and accepted June 24, 2012.

Published online June 24, 2012
10.1021/nn3020695

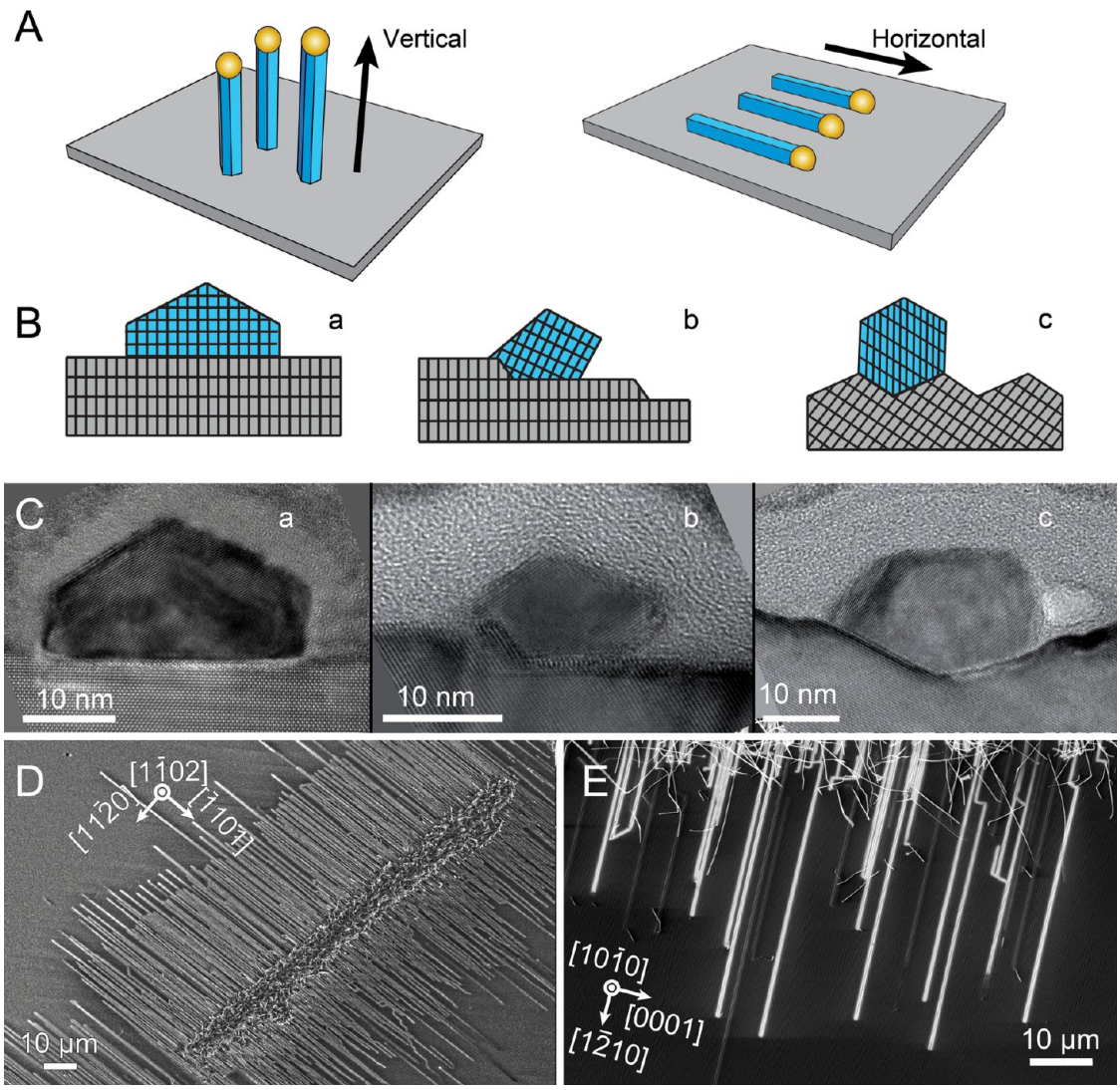

Figure 1. Guided growth of horizontal nanowires: Concept and realization. (A) Schematic view of guided VLS growth (right) *vs* conventional VLS growth (left). (B) Three modes of guided VLS growth (schematic cross-section views): (a) epitaxial growth along specific lattice directions, (b) graphoepitaxial growth along L-shaped nanosteps of an annealed miscut substrate, and (c) graphoepitaxial growth along V-shaped nanogrooves of an annealed unstable low-index substrate. (C) Experimental realization of (B) for ZnO nanowires on different planes of sapphire (cross-sectional TEM images): (a) R(1$\bar{1}$02), (b) annealed miscut C(0001)by 2° toward [$\bar{1}$100], and (c) annealed M (10$\bar{1}$0). (D) Dense, perfectly parallel, ZnO nanowire arrays grown on R(1$\bar{1}$02) sapphire. (E) Perfectly aligned GaN nanowires grown on annealed M-plane sapphire.

GaN[31] and GaAs nanowires on GaAs(100).[32] In these cases, the alignment was induced by a single epitaxial relation, and hence the possibility of controllably varying the crystallographic orientation of the nanowires was not demonstrated. A further development of this concept was the work done by our group on the guided growth of GaN on sapphire.[33] In this recent work, we used different sapphire substrates to guide millimeter-long nanowires using both epitaxy and the strong guiding effect of surface steps and grooves, known as graphoepitaxy.[34] Using different planes of sapphire, including both flat surfaces and faceted surfaces with nanosteps and nanogrooves, we could control the crystallographic orientations of the nanowire while achieving perfect alignment in different geometries. Despite their interaction with the surface, the guided nanowires showed excellent optical and electronic properties, indicating a low concentration of defects. This paved the way to highly controlled nanowires structures with potential applications not available by other means. However, the generality of the guided growth phenomenon was not demonstrated for other materials besides GaN.

Here we demonstrate the generality of the guided growth approach by reporting the guided growth of ZnO nanowires with controlled orientations on various flat and faceted sapphire surfaces. On the basis of our previous results with GaN, we postulated three general modes of guided VLS growth of horizontal nanowires, depending on the substrate morphology, as depicted in Figure 1B: (a) epitaxial growth along specific lattice directions, driven by minimization of interfacial energy

and strain; (b) graphoepitaxial growth along L-shaped nanosteps spontaneously formed upon annealing a miscut substrate, driven by maximization of the interface area between the substrate and the nanowire or the catalyst; and (c) graphoepitaxial growth along V-shaped nanogrooves spontaneously formed upon annealing an unstable low-index surface, driven similarly to (b). Sapphire (α-Al_2O_3) is a trigonal crystal of the $R\bar{3}c$ space group. Its equilibrium Wulff shape is characterized by facets C{0001}, R{1$\bar{1}$02}, S{10$\bar{1}$1}, P{11$\bar{2}$3}, A{11$\bar{2}$0}, and M{10$\bar{1}$0} (too unstable to be present), in order of increasing surface energy.[35] Thus, when sapphire substrates with unstable orientations, such as M-plane or miscut C-plane, are annealed at a high temperature, they spontaneously become periodically faceted. Thus, sapphire provides us with a series of flat and faceted surfaces suitable for these modes of guided growth.

In this article, we describe the guided growth of horizontal ZnO nanowires on eight different flat and faceted sapphire substrates, displaying the three different modes of guided growth. This is the first demonstration of guided ZnO nanowire growth on faceted substrates with nanosteps and nanogrooves and on three different flat sapphire substrates (specifically, C-, R-, and M-planes). We characterize the crystallographic orientation of the ZnO nanowires and the epitaxial and graphoepitaxial effects that lead to their guided growth. We also examine the optical properties of the nanowires using photoluminescence and the electronic properties of the nanowires by building single-nanowire field-effect transistors. Finally, we compare the guided growth of ZnO nanowires with that of GaN nanowires. The similarities and differences between these two materials reveal the general principles underlying the guided growth phenomenon.

RESULTS AND DISCUSSION

We grew guided ZnO nanowires on eight different sapphire substrates: C{0001}, R{1$\bar{1}$02}, A{11$\bar{2}$0}, M{10$\bar{1}$0}, annealed M{10$\bar{1}$0}, and annealed miscut C{0001} planes tilted by 2° toward [11$\bar{2}$0], [1$\bar{1}$00], and [$\bar{1}$100]. The growth was carried out by the vapor–liquid–solid (VLS) method in a quartz tube inside a tube furnace with fast heating capabilities (25–1000 °C in 5 min). The Zn and O elements were supplied from ZnO powder mixed with carbon powder (1:1 mass ratio), held at 1000 °C, while the samples are held downstream at a temperature of 900 °C. The Au catalyst was patterned by photolithography. Au catalyst nanoparticles were created either by electron-beam evaporation of a thin (1 nm) layer, followed by dewetting at elevated temperature, or by dispersion of commercially purchased Au colloids of different sizes (see Methods section). After VLS growth, the bulk of the catalyst patterns was covered with dense forests of vertically grown ZnO nanowires and nanobelts, whereas a large number of nanowires grew horizontally from the pattern edges, extending onto the clean sapphire surface. Sonication for a few seconds in isopropyl alcohol removes the nanowire forests, leaving only the horizontal nanowires in place. The typical nanowire thickness, d (defined here as their top-projection width), varied with the catalyst particle diameter, ranging between 5 and 50 nm. The nanowire lengths could be up to 50 μm. In most cases, the nanowires developed a slightly tapered shape during the synthesis, presumably due to direct addition of material from the vapor phase to the nanowire sidewalls. The crystallographic structure, orientation, and epitaxial relations of the nanowire on the substrate were elucidated by cutting thin (50–100 nm) slices across the nanowires using a focused ion beam (FIB) and observing them under a high-resolution transmission electron microscope (HRTEM). Low-magnification images (Figure 1C) confirm the postulated modes of guided growth (Figure 1B). Further magnification enabled us to identify the specific crystallographic and epitaxial details of each nanowire. The crystallographic orientations and epitaxial relations for the ZnO nanowires on all of the sapphire surfaces are summarized in Table 1. The mismatch is presented for both room temperature (25 °C) and growth temperature (900 °C), although the change with temperature is usually much smaller than the mismatch itself. The following paragraphs describe the guided growth of horizontal ZnO nanowires on the different sapphire substrates, in order of decreasing symmetry.

Guided ZnO Nanowires on C (0001) and Annealed Miscut C (0001) Sapphire. The growth of ZnO nanowires on C-plane sapphire and on annealed miscut C-plane sapphire allows us to observe two of our postulated modes of guided growth (Figure 2) and highlight the graphoepitaxial effect. On well-cut C-plane, nanowires grow along the six isomorphic ⟨11$\bar{2}$0⟩ directions defined by the three-fold symmetry of the C-plane and the three {11$\bar{2}$0} glide planes. This symmetry causes the guided wires to create a triangular network (Figure 2B). The planar epitaxial relations are $(0001)_{ZnO} \| (0001)_{Al_2O_3}$, as reported for 2D films.[36] The nanowire growth directions are $[10\bar{1}0]_{ZnO} \| [11\bar{2}0]_{Al_2O_3}$, while across the nanowire, the relations are reversed: $[11\bar{2}0]_{ZnO} \| [10\bar{1}0]_{Al_2O_3}$ (Table 1). The lattice mismatch is 18.2% in the growth direction and −1.49% across the nanowire. This contradicts the intuitive assumption that the nanowire would prefer to grow in the direction of lowest mismatch, as in the case of some other sapphire substrates (Table 1). However, what determines the nanowire growth direction is the overall minimization of the strain energy, including various relaxation mechanisms, as previously suggested.[37]

When C-plane sapphire is miscut to a high-index plane, the annealing of the sapphire substrate produces a surface with a periodic array of L-shaped nanosteps (Figure 2A).[38] When the C-plane is miscut by 2° toward [1$\bar{1}$00] or toward [$\bar{1}$100], the ZnO

TABLE 1. Epitaxial Relations and Lattice Mismatch for Guided ZnO Nanowires on Different Sapphire Surfaces (Nanowire Axial Orientations Are Highlighted Bold; XXXX Indicates Variable Orientations)

					mismatch at 25 °C (%)[a] (mismatch at 900 °C (%))[a]	
substrate orientation	# of NWs	horizontal ZnO|| Al_2O_3	axial ZnO|| Al_2O_3	transversal ZnO|| Al_2O_3	axial	transversal
C (0001)	5	(0001)|| (0001)	**[10$\bar{1}$0]**\|\| [11$\bar{2}$0]	[1$\bar{2}$10]\|\| [1$\bar{1}$00]	18.20 (18.22)	−1.49 (−1.47)
annealed miscut C (0001)	10	(10$\bar{1}$1)|| (0001)	**[11$\bar{2}$3]**\|\| [11$\bar{2}$0]	[$\bar{2}$3$\bar{1}$1]\|\| [1$\bar{1}$00]	3.10 (2.25)	5.06 (5.08)
	8	(XXXX)|| (0001)	**[XXXX]**|| [11$\bar{2}$0][b]	[XXXX]|| [1$\bar{1}$00]		
A (11$\bar{2}$0)	16	(0001)|| (11$\bar{2}$0)	**[10$\bar{1}$0]**\|\| [1$\bar{1}$00]	[1$\bar{2}$10]|| [0001]	2.36 (2.38)	0.02 (−0.05)
R (1$\bar{1}$02)	24	(1$\bar{2}$10)\|\| (1$\bar{1}$02)[c]	**[0001]**|| [$\bar{1}$101]	[10$\bar{1}$0]\|\| [11$\bar{2}$0][c]	1.49 (1.12)	18.20 (18.22)
M (10$\bar{1}$0) (d = 25−50 nm)	7	(1$\bar{1}$00)\|\| (10$\bar{1}$0)	**[0001]**|| [1$\bar{2}$10]	[11$\bar{2}$0]|| [0001]	9.34 (9.04)	0.02 (−0.05)
M (10$\bar{1}$0) (d < 25 nm)	22	(1$\bar{1}$00)\|\| (10$\bar{1}$0)	**[11$\bar{2}$0]**|| [0001]	[0001]|| [1$\bar{2}$10]	−2.54 (−2.63)	9.34 (9.04)
annealed M (10$\bar{1}$0)[d]	12	(11$\bar{2}$0)\|\| (1$\bar{1}$02)[d]	**[1$\bar{1}$00]**\|\| [11$\bar{2}$0][d]	[0001]|| [$\bar{1}$101]	18.20 (18.22)	1.49 (1.12)

[a] From refs 56 and 57. [b] Miscut toward [1$\bar{1}$00] or [$\bar{1}$100]. [c] The $(11\bar{2}0)_{ZnO}$ planes are tilted by 6°, as explained in the text. [d] Epitaxial relations are stated with respect to the R-plane nanofacets formed after annealing M-plane sapphire, as explained in the text and Figure 7.

nanowires choose to grow only along two directions ±[11$\bar{2}$0], forming parallel arrays (Figure 2C,D). Here, the VLS growth is clearly guided by the L-shaped nanosteps (Figure 2G). Furthermore, when the C-plane is miscut by 2° toward [11$\bar{2}$0], the ZnO nanowires are coerced to grow along the ±[1$\bar{1}$00] directions of the steps (Figure 2E), at 30° from the growth directions preferred by the nanowires on the well-cut C-plane. Clearly, the graphoepitaxial guiding effect overrules the epitaxial lattice guiding effect. Surprisingly, the graphoepitaxial effect due to the presence of nanosteps affects not only the growth direction on the ZnO nanowires but also their crystallographic orientation. On flat C-plane sapphire, the ZnO nanowires grow with the (0001) plane parallel to the substrate surface, but when the same plane is miscut, they grow with their (10$\bar{1}$1) plane parallel to the substrate surface. This remarkable graphoepitaxial effect also causes the wire to grow in an unusual $[11\bar{2}3]_{ZnO}$ semipolar orientation, in contrast to the usual nonpolar $[10\bar{1}0]_{ZnO}$ orientation of guided ZnO nanowires on well-cut C-plane sapphire.

On annealed miscut C-plane sapphire miscut toward [1$\bar{1}$00] and toward [$\bar{1}$100], we mostly encountered the same epitaxial relation as on annealed miscut C-plane sapphire miscut toward [11$\bar{2}$0], but less frequently, we also found other orientations (Table 1 and Supporting Information). This variability may be related to the fact that, along the steps, the nanowires have to accommodate two incompatible epitaxial relations, one with the "tread" facet and the other with the "riser" facet of the nanosteps.

Guided ZnO Nanowires on A (11$\bar{2}$0) Sapphire. The A-plane sapphire has already been used as a substrate for the epitaxial growth of horizontal ZnO nanowires,[30] with a low crystallographic mismatch, lower than the mismatch of ZnO with any other crystallographic plane of sapphire (Table 1). Horizontal ZnO nanowires grow on A-plane sapphire in two opposite directions $\pm[1\bar{1}00]_{Al_2O_3}$, as shown in Figure 3A. We found the epitaxial relations to be identical to those reported for thin films (Table 1).[36] The nanowires grow in the nonpolar, $[10\bar{1}0]_{ZnO}$ direction, similar to the previous reports.[30,37] The lattice mismatch is 2.36% in the growth direction and 0.02% across the nanowire.

A common feature visible in TEM images (Figure 3B) is the restructuring of the substrate: The nanowire seems to be slightly indented into the substrate surface, while the latter displays lifted outer rims. This restructuring may be driven by minimization of the interface energy and strain between nanowire and substrate material, as previously suggested.[37]

Guided ZnO Nanowires on R (1$\bar{1}$02) Sapphire. We grew guided horizontal ZnO nanowires on R-plane sapphire (Figure 1D and Figure 4), obtaining similar epitaxial relations to those previously reported ZnO nanonecklaces on R-plane sapphire,[39] although in our experimental conditions, we were able to achieve smooth, uniform nanowires (Figure 4C). The nanowires grow in two opposite directions $\pm[\bar{1}101]_{Al_2O_3}$, forming dense combs (Figure 4A). Nanowire arrays grow as dense as 8 nanowires/μm with perfectly parallel directions (Figure 4B). In this case, the nanowires grow with a polar $[0001]_{ZnO}$ growth axis (Table 1). The lattice mismatch is 1.49% in the growth direction and 18.2% in the transversal direction.

In fact, TEM images (Figure 4C,D) of 24 nanowires reveal that the actual epitaxial relations slightly deviate from those written above: The (0001) planes of the ZnO are not perfectly normal to (1$\bar{1}$02) sapphire surface but are tilted by 6°. This tilt reduces the mismatch between nanowire and substrate by a factor of cos α, where α is the tilt angle with respect to the surface normal. The mismatch is thus slightly reduced from 18.2 to 17.5%. This mismatch is then further diminished by the formation of periodic misfit dislocations in the interface between nanowire and substrate. Frequency-filtered FFT images of nanowires on R-plane sapphire (Figure 4F) reveal that the misfit dislocations appear every 5 or 6 ZnO lattice fringes, in accordance with the calculated mismatch.

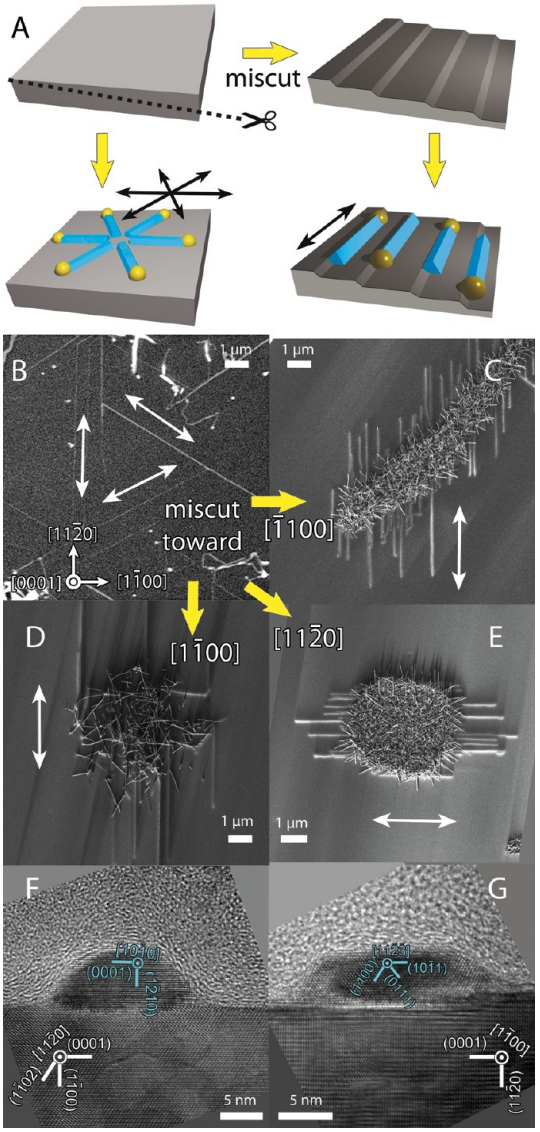

Figure 2. Graphoepitaxial effect on the guided growth of horizontal ZnO nanowires on C-plane sapphire. (A) Graphoepitaxial effect on C-plane sapphire (schematic). (B–E) Corresponding scanning electron microscope (SEM) images showing how the guided growth of ZnO nanowires changes from six directions on well-cut C-plane (B) to bidirectional growth by the introduction of nanosteps when the substrate is miscut toward [$\bar{1}$100] (C), [1$\bar{1}$00] (D), and [11$\bar{2}$0] (E). (F) Cross-sectional TEM image of a nanowire growing on well-cut C plane in the [11$\bar{2}$0]$_{Al_2O_3}$ direction. (G) Cross-sectional TEM image of a ZnO nanowire graphoepitaxially guided along a L-shaped nanosteps, on annealed C-plane sapphire miscut 2° toward [11$\bar{2}$0].

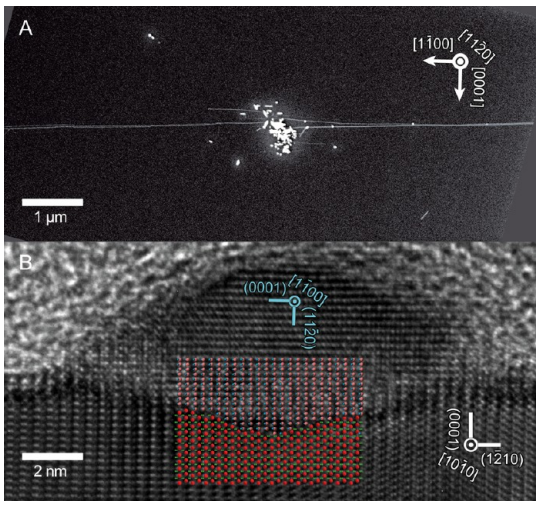

Figure 3. Guided ZnO nanowires on A-plane sapphire. (A) SEM image showing bidirectional growth of horizontal ZnO nanowires from patterned catalyst. (B) Cross-sectional TEM image of a ZnO nanowire growing in the [1$\bar{1}$00]$_{Al_2O_3}$ direction. The substrate is clearly reconstructed around the nanowire to minimize the interface energy and strain between nanowire and substrate.

Guided ZnO Nanowires on M (10$\bar{1}$0) Sapphire. On M-plane sapphire, ZnO nanowires grow in four perpendicular directions: $\pm$[1$\bar{2}$10]$_{Al_2O_3}$ and $\pm$[0001]$_{Al_2O_3}$. Surprisingly, the width of the nanowires dictates their growth direction (Figure 5). Diameter-dependent crystallographic orientations had only been reported for off-plane nanowires. For example, the crystallographic axis of off-plane epitaxial silicon nanowires on Si(100) has been shown to change from the [111] to the [110] direction when catalyst size is smaller or larger than 20 nm, respectively.[40] In our present case, all of the ZnO nanowires grown on M-plane sapphire possess the same planar epitaxial relations (Table 1), but the growth direction of the nanowires changes by 90° depending on their thickness. Thin nanowires (d = 5–25 nm) grow with a nonpolar [11$\bar{2}$0]$_{ZnO}$ orientation along the $\pm$[1$\bar{2}$10]$_{Al_2O_3}$ directions (Figure 5B,C,E), whereas thick (d = 25–50 nm) nanowires grow with a polar [0001]$_{ZnO}$ orientation along $\pm$[0001]$_{Al_2O_3}$ directions (Figure 5D,F). In the case of thin nanowires, the lattice mismatch is 0.02% in the growth direction and 9.34% in the transversal direction. For thick nanowires, the mismatch values are reversed. We attribute the transition between these two regimes to the critical thickness for misfit dislocations: For thin nanowires (d = 5–25 nm), strain simply leads to lattice expansion, and the direction that is least strained is the [11$\bar{2}$0]$_{ZnO}$ direction, which accordingly becomes the growth direction. As the thickness of the nanowire increases beyond the critical value (≈25 nm), the formation of misfit dislocations becomes more energetically favorable than lattice expansion. In this regime, strain in the [0001]$_{ZnO}$ direction is effectively relieved by the formation of misfit dislocations and becomes less strained than the [11$\bar{2}$0]$_{ZnO}$ direction. As a result, the [0001]$_{ZnO}$ direction becomes the preferred growth direction.

This thickness-dependent growth enables us to choose the growth of nanowires with polar or nonpolar orientations on the same substrate. Our group has already demonstrated polarity-controlled growth of guided nanowires by choosing different substrate orientations,[33] but here we show for the first time control of both polarity and growth direction on the

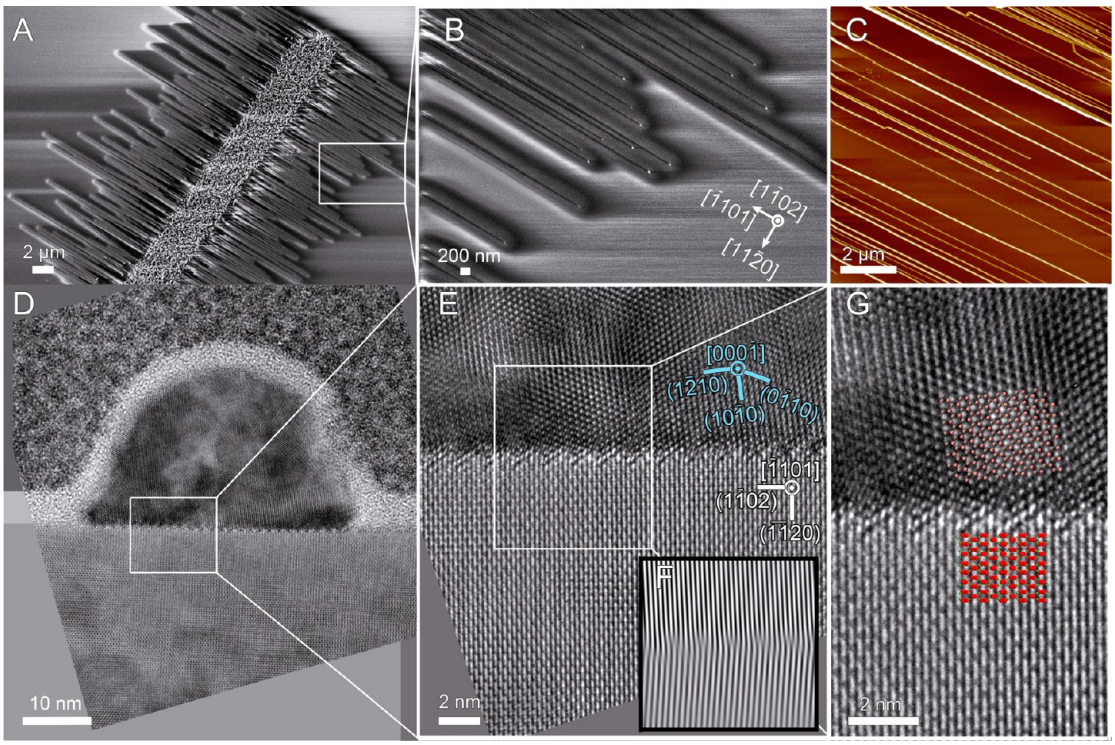

Figure 4. Guided ZnO nanowires on R-plane sapphire. (A) SEM image showing bidirectional, dense growth of horizontal ZnO nanowires from patterned catalyst. (B) Larger magnification of the area indicated by the white box. The Au catalyst is visible at the end of the nanowires. (C) AFM image of ZnO nanowires on R-plane sapphire, showing perfect alignment and smooth sidewalls. (D) Cross-sectional TEM image of a nanowire growing in the $[0001]_{ZnO}$ direction. (E,G) Larger magnification of the indicated area, showing possible atomic locations. (F) Fourier-filtered version of D, highlighting the relief of strain *via* periodic misfit dislocations, and the 6° angle between the lattice fringes of substrate and nanowire.

same substrate. This polarity control could be important for various applications, such as nonlinear optics or LEDs (*vide infra*).

TEM images (Figure 5B) reveal that very thin nanowires (≈7 nm) usually have a "hut-shaped" cross section composed of three different grains: one central grain and two grains capping it from left and right, creating the two halves of the hut's "roof". All three grains grow in the same $[11\bar{2}0]_{ZnO}$ crystallographic direction but are rotated around the growth axis differently: The central grain has its $(0001)_{ZnO}$ planes normal to the substrate, whereas the left and right "roof" halves have their $(0001)_{ZnO}$ planes at +60° and −60° with respect to the central grain. The $(0001)_{ZnO}$ planes of the central grain match the $(11\bar{2}0)_{Al_2O_3}$ planes, while the left and right "roof" halves match their $(0001)_{ZnO}$ planes to the symmetrically equivalent $(\bar{2}110)_{Al_2O_3}$ and $(1\bar{2}10)_{Al_2O_3}$, respectively. The driving force for this multidomain formation could be the tendency of the ZnO nanowires to expose (0001) facets: With only one grain, a large amount of the nanowire surface would expose a ZnO $(10\bar{1}0)$ facet. By creating three grains, the nanowire can expose (0001) facets almost exclusively. This result is surprising considering the high energy of the $(0001)_{ZnO}$ planes.[41] However, vertical ZnO nanowires growing in the same $[11\bar{2}0]_{ZnO}$ direction and exhibiting only $(0001)_{ZnO}$ and $(000\bar{1})_{ZnO}$ facets have been reported and rationalized as products of kinetically controlled growth.[42] Slightly thicker nanowires (d = 10−25 nm) adopt similar orientations (Figure 5C,E) but are composed of a single grain, probably due to the increasing energetic cost of grain boundary formation for thicker nanowires. Although all of these single-grain nanowires have the same nonpolar axial orientation, $[11\bar{2}0]_{ZnO}$, their transversal orientation can vary as the $(0001)_{ZnO}$ planes match either of the equivalent $(11\bar{2}0)$ planes of the sapphire (Supporting Information). Since the high-energy $(0001)_{ZnO}$ planes show increased reactivity, for example, toward CO adsorption,[43] these nanowires could be more efficient than other nanowires for different applications, such as CO detectors.

Guided ZnO Nanowires on Annealed M $(10\bar{1}0)$ Sapphire. Sapphire M-plane is thermodynamically unstable and undergoes faceting at elevated temperatures.[38] The resulting surface is composed of two types of facets: S-plane facets and R-plane facets, as shown in Figure 6C. This periodically faceted surface forms a series of grooves that guide the growth of ZnO nanowires by a graphoepitaxial effect (Figure 6A,B). The nanowires grow on annealed M-plane in the same $[11\bar{2}0]_{Al_2O_3}$ direction as the thick (d = 25−50 nm) nanowires on non-annealed M-plane. However, this graphoepitaxial effect enables us to grow nanowires of any thickness in

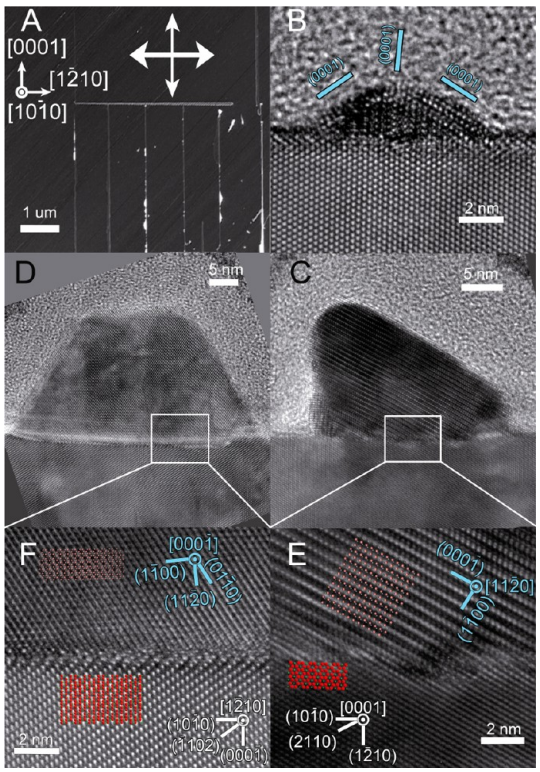

Figure 5. Thickness-dependent guided growth of horizontal ZnO nanowires on M-plane sapphire. (A) SEM image, showing two perpendicular growth directions. (B) Cross-sectional TEM image of a thin ZnO nanowire (d < 8 nm) growing in the $[11\bar{2}0]_{Al_2O_3}$ direction, exhibiting a "hut" shape. (C) Cross-sectional TEM image of a thicker ZnO nanowire (d = 10−25 nm) growing in the $[11\bar{2}0]_{Al_2O_3}$ direction. (D) Cross-sectional TEM image of a thick (d > 25 nm) ZnO nanowire growing in the Al_2O_3 [0001] direction. (E,F) Larger magnification of the indicated areas in (D) and (C), showing possible atomic locations.

this direction. Furthermore, the epitaxial relations are different from those of nanowires that grow on M-plane sapphire. On the faceted surface of annealed M-plane sapphire, the graphoepitaxial effect controls the growth direction of the nanowires along the nanofacets, while the R-plane orientation of the nanofacets dictates the crystallographic orientation of the ZnO nanowires. Consequently, instead of growing in the $[\bar{1}101]_{Al_2O_3}$ direction as on flat R-plane sapphire, the nanowires grow along the nanogrooves in the $[11\bar{2}0]_{Al_2O_3}$ direction, which is rotated by 90° (Figure 7). With respect to the R-plane nanofacets, the nanowires show exactly the same epitaxial relation as nanowires grown on flat R-plane sapphire, but the nanowire axis is changed from the polar $[0001]_{ZnO}$ orientation to the nonpolar $[1\bar{1}00]_{ZnO}$ orientation. This rotation may seem surprising considering that the nanowires grow in a direction with a large mismatch of 18.2%, compared to nanowires that grow on flat R-plane, where the mismatch in the growth direction is −1.49% (Table 1). This underscores to what extent the graphoepitaxial effect overrules the epitaxial effect.

When inspecting graphoepitaxial ZnO nanowires on annealed M-plane sapphire in the TEM (Figure 6D),

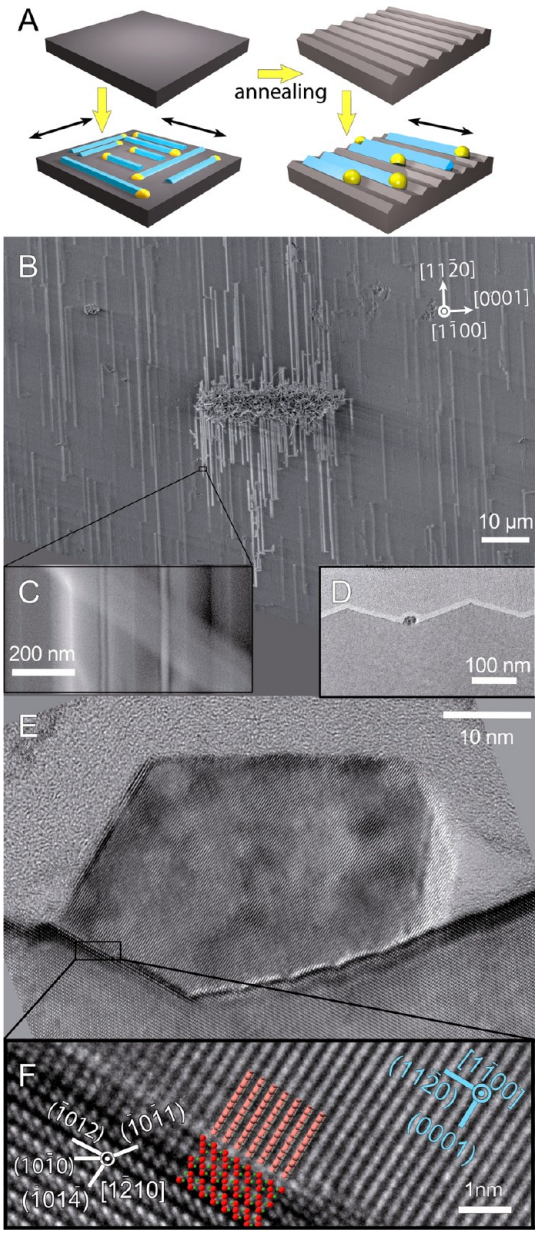

Figure 6. Graphoepitaxially guided growth of ZnO nanowires on annealed M-plane sapphire. (A) Graphoepitaxial effect on M-plane sapphire (schematic). (B) SEM image of dense ZnO nanowires growing from a patterned and dispersed Au nanoparticles. (C) Magnification of the indicated area, showing the nanowires guided by the grooves of the surface. (D) Low-magnification cross-sectional TEM image of ZnO nanowire, showing the position of the nanowire in the grooves. (E) Cross-sectional TEM image of a ZnO nanowire growing in the $[1\bar{2}10]_{Al_2O_3}$ direction. (F) Larger magnification of the indicated area, showing possible atomic locations.

the substrate shows at least two directions of fringes, as usual, but the ZnO nanowires show only one direction of lattice fringes. The observed fringes correspond to the (0006) planes of ZnO, while the expected $(11\bar{2}0)_{ZnO}$ fringes are missing. This indicates that the nanowire $(11\bar{2}0)_{ZnO}$ plane is tilted with respect to the substrate plane. This tilt is directly related to the 6° tilt observed in the guided ZnO nanowires on well-cut

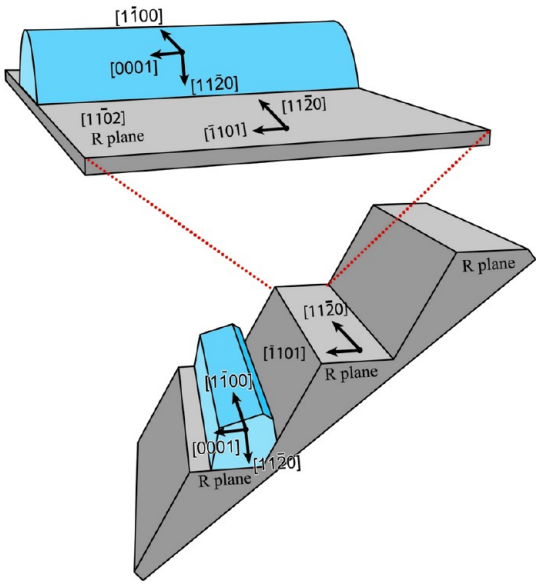

Figure 7. Growth of ZnO nanowires on singular R-plane sapphire *vs* the graphoepitaxially directed growth on the R-plane facets of annealed M-plane sapphire (schematic representation). The epitaxial relations are identical for the two cases (with respect to the sapphire R-plane). However, on R-plane, the nanowires grow in the $[1\bar{1}01]_{Al_2O_3}$ direction, and on the R-plane facets of annealed M-plane sapphire, the nanowires grow in the $[11\bar{2}0]_{Al_2O_3}$ direction due to the graphoepitaxial effect.

R-plane sapphire between the $(11\bar{2}0)_{ZnO}$ planes and the $(11\bar{2}0)_{Al_2O_3}$ planes (Figure 4D). The difference is that on R-plane sapphire the tilt is across the nanowire axis, whereas on annealed M-plane, the tilt is toward the nanowire axis. Hence, the nanowire orientation is not exactly $[1\bar{1}00]_{ZnO}$, as shown in Table 1, but a vicinal orientation 6° off $[1\bar{1}00]_{ZnO}$ toward $[11\bar{2}0]_{ZnO}$. This is, to the best of our knowledge, the first observation of nanowires with a vicinal orientation.

Optical Properties of the Guided ZnO Nanowires. Previous studies in our group have shown that guided GaN nanowires exhibit excellent optical properties, similar to vertically grown GaN nanowires,[33] refuting initial concerns that the interaction with the substrate might induce strain-related defects that would degrade their optical and electronic properties. Here we show that guided ZnO nanowires also exhibit excellent optical properties, similar to those of freestanding ZnO nanowires. We characterized the optical properties by measuring the photoluminescence (PL) of single ZnO nanowires on different substrates using a confocal microscope with a He−Cd laser (Figure 8). The PL spectra are typical of high-quality ZnO nanowires with a single PL peak in the range of 328−745 nm.[44] Notably, we did not see any green emission typical of defective ZnO.[45,46] The peaks of the photoluminescence were varied slightly between the different substrates, with λ_{max} values between 374 and 384 nm. We cannot attribute the observed variation in λ_{max} to quantum confinement because the exciton Bohr radius of bulk

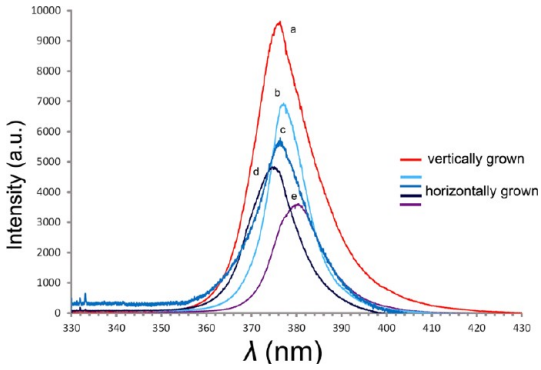

Figure 8. Optical properties of guided ZnO nanowires. Typical single-nanowire photoluminescence spectra at room temperature of (a) ZnO nanowires vertically grown on annealed M-plane sapphire dispersed on A-plane sapphire. (b) Thick (d = 25−50 nm) horizontally grown ZnO nanowires on M-plane sapphire. (c) Horizontally grown ZnO nanowires on R-plane sapphire. (d) Thin (d = 10−25 nm) horizontally grown ZnO nanowires on M-plane sapphire. PL peak is blue-shifted ~2.5 nm with respect to the thicker nanowires growing in 90°, on the same substrate, at the same synthesis. (e) Horizontally grown ZnO nanowires on annealed M-plane sapphire. Excitation wavelength λ_{ex} = 325 nm.

ZnO is 2.34 nm, that is, smaller than the radius of the narrowest nanowire we were able to measure. Therefore, we suggest that the variation in the PL peak position may result from the different amounts of strain accumulated in the nanowires, according to the size of the nanowires and the substrate on which they grow.[47] Furthermore, we observed a small but consistent difference of 2 nm between the two kinds of nanowires growing in two different directions on M-plane sapphire. The thicker nanowires growing with a polar $[0001]_{ZnO}$ direction showed a PL peak at λ_{max}= 376 (Figure 8d), and the thinner nanowires growing in the nonpolar $[11\bar{2}0]_{ZnO}$ direction showed a PL peak at λ_{max}= 374 (Figure 8e). Since these nanowires grew at the same time under the same conditions, this difference cannot be a result of changes in composition or unintentional doping, but may be attributed to the different accumulated strain in these nanowires, as suggested. For reference, we also measured the PL spectra of nanowires vertically grown in the same conditions and dispersed onto the same substrate (Figure 8a). We found the photoluminescence spectra of horizontally grown guided nanowires to be very similar to those of vertical nanowires, indicating that the interaction with the substrate does not induce defects that degrade the optical properties of the guided ZnO nanowires.

Electronic Properties of the Guided ZnO Nanowires. Another property that may be strongly affected by defects is the charge carrier mobility. We characterize the electronic properties of the horizontal epitaxial ZnO nanowires by building single-nanowire field-effect transistors (Figure 9, inset) with top gates. The nanowires display n-type behavior (Figure 9A,B) with mobility μ = 15−66 $cm^2/(V \cdot s)$ and electron density $n_e = 1.6 \times 10^{19}$ to

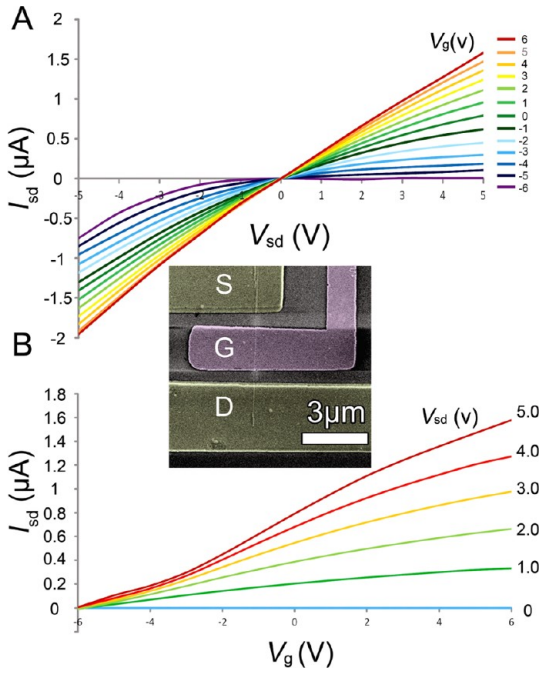

Figure 9. Electronic properties of guided ZnO nanowires. Electrical characterization of guided ZnO nanowires was performed in a single-nanowire FET configuration at room temperature. (A) Source−drain current (I_{sd}) *vs* source−drain voltage (V_{sd}) are displayed for different gate voltages (V_g). Inset: SEM image of a typical FET device, showing the nanowire, electrodes, and top gate. (B) $I_{sd}-V_g$ curves for different V_{sd} bias voltages. The charge carrier density can be extracted from the linear part of the graphs. The electrical measurements were performed on nanowires horizontally grown on R-plane sapphire.

2.6×10^{19} cm^{-3}. These values are comparable with those reported for nonhorizontally grown ZnO nanowires.[48]

Comparison between Guided ZnO and GaN Nanowires on Sapphire. The present work demonstrates the generality of the guided growth approach and allows us to further learn about the guided growth phenomenon by comparing the guided growth of ZnO nanowires to the growth of GaN nanowires on sapphire.[33] Both ZnO and GaN nanowires show horizontal growth on sapphire, and both display the same three modes of guided growth (Figure 1B). Although ZnO is a II−IV material and GaN is a III−V, with different lattice parameters, both ZnO and GaN exhibit the same ability to grow horizontally along specific directions on any of the eight examined sapphire substrates (Table 1). Thus, the guided growth of horizontal nanowires shows a large general tolerance for high mismatch, compared with 2D films. We attribute this tolerance to the 1D nature of the nanowires, where stress accumulates only in one direction but can relax sideways (see discussion below). The most notable differences between guided ZnO and GaN nanowires are:

(a) The morphologies of the ZnO and GaN nanowires horizontally grown on sapphire are usually similar. However, GaN nanowires grown on flat substrates had exclusively nonpolar axes, while ZnO nanowires grown on flat sapphire show either polar or nonpolar axes (*e.g.*, on R-plane sapphire, ZnO nanowires grow with a polar axis, whereas GaN nanowires grow with a nonpolar axis). This observation shows that polarity does not play a role in guiding the growth of ZnO and GaN nanowires on sapphire. Interestingly, both ZnO and GaN nanowires grow on annealed miscut C-plane sapphire with semipolar orientations.

(b) The growth direction of ZnO nanowires on M-plane sapphire depends on the nanowire thickness, whereas the guided growth of GaN did not show thickness dependence. At a critical thickness, misfit dislocations relieve stress such that the least stressed crystal direction is changed; this may be unique to ZnO.

(c) Guided growth of GaN nanowires on M-plane and R-plane sapphire is unidirectional, whereas ZnO nanowire growth on these substrates is bidirectional. In both GaN and ZnO, we observed a relationship between the nanowire growth directions and the symmetry of the substrate plane. Flat substrates with D_3, C_2, or D_1 morphological symmetries lead to epitaxial nanowire growth along six, two, and one single direction, respectively. In the case of D_1 symmetry, as in R- and M-plane sapphire, GaN nanowires grow unidirectionally and ZnO grows in both directions. However, when looking closely at ZnO nanowires grown on R-plane sapphire or M-plane sapphire under certain conditions, it is possible to see that there is still a statistically preferred growth direction (see Supporting Information Figure S9). This preferred direction, however, is less selective than for guided GaN nanowires, so that under our usual synthetic conditions ZnO nanowires grow in two opposite directions.

(d) ZnO nanowires on sapphire show, in most cases (see Table 1), only one orientation per substrate plane, while GaN showed, in many cases, several alternatives. This could be due to more pronounced energetic minima for each preferred orientation of ZnO. GaN might have several close minima for each orientation, promoting some degree of variability. For example, the epitaxial relations of ZnO nanowires grown on annealed M-plane are constant, whereas in GaN nanowires, they are variable. This is probably because it is energetically preferable for ZnO to match the R-plane facets and not the S-plane facets (Figure 6D), while for GaN, the energetic difference between matching the S-plane and the R-plane is small, and hence the wire can rotate to match either of the two facets.

On the basis of all of these observations, we conclude that the guided growth of horizontal nanowires has a much higher mismatch tolerance than 2D film heteroepitaxy. We expect to see this tolerance in other materials and substrate, perhaps enabling high-quality

heteroepitaxial growth not available by other means. The reason for this tolerance is that whereas in a 2D film stress accumulates in two directions, in a nanowire, stress accumulates along its axis but can easily relax in the nanoscopic transversal direction by expansion, compression, or localized misfit dislocations. This makes the 1D system much more tolerant to mismatch than a 2D film. Furthermore, unlike other methods that produce 1D nanostructures, like epitaxial lateral overgrowth,[49] here the nanowire nucleates only from the metal catalyst droplet and therefore grows free of grain boundaries.

The exact mechanism of guided VLS growth is still not fully understood. A recent theoretical model predicts horizontal VLS growth of nanowires, on the basis of catalyst droplet statics and the formation and growth of nanowire facets.[50] This model appears to be highly relevant to our results, but as a continuum model, it does not refer to the epitaxial relation between the nanowire material and the substrate. To explain and predict the orientation control in our results, a more detailed model will be required. To this end, a few important observations need to be taken into account: First, the epitaxial relations of most of our nanowires are consistent with those reported in literature for thin films produced by different methods.[36] This suggests a significant degree of thermodynamic control. On the other hand, we have observed nanowire facets that are not the lowest energy facets. This suggests also a significant degree of kinetic control. Second, we need to address the control of the growth direction. We propose that several factors, acting in cooperation or competition, could determine the growth direction. In the simple case of homoepitaxy,[32] where GaAs nanowires are horizontally grown on GaAs, there is obviously no strain in any direction. However, the nanowires are guided and grow in a specific direction. This could be due to kinetics of crystal growth, the surface energies of the different crystal surfaces, or due to energetics of crystal nucleation. In the more complex case of heteroepitaxy, such as the guided growth of GaN and ZnO on sapphire, the strain is anisotropic, and its influence may compete or add to the previous guiding effects. Furthermore, we have also seen that the strain is sometimes thickness-dependent. All of these influencing terms may also depend on temperature, pressure, and other synthetic conditions. Although a full theoretical model is beyond the scope of this article, we are providing a rich set of data and considerations for the development of such model.

CONCLUSIONS

We have demonstrated the guided growth of horizontally aligned ZnO nanowires on different flat and faceted surfaces of sapphire, proving the three postulated guided growth modes: (a) epitaxial growth along specific lattice directions, (b) graphoepitaxial growth along nanosteps, and (c) graphoepitaxial growth along nanogrooves. Our results show that the guided VLS growth enables us to control the crystallographic orientation and growth morphology of aligned ZnO nanowires on sapphire. The growth morphologies include six, four, or two growth directions, which match the morphological symmetry of the substrates. The crystallographic alignment, verified in more than 100 nanowires, includes nanowires with polar [0001], semipolar [$11\bar{2}3$], or nonpolar [$10\bar{1}0$] and [$11\bar{2}0$] growth directions. This could have great technological implications since the polarity of semiconducting nanowires and thin films was found to affect their photophysical properties due to internal fields.[51] Epitaxial VLS growth on different substrates has enabled the selective production of polar and nonpolar nanowires as vertical arrays, but no available postgrowth method based on dispersions can horizontally align them with coherent polarity, whereas guided growth could yield coherently oriented nanowires with similar polarity. This polarity control may have important advantages in photonic, optoelectronic, and high-frequency applications, as well as in nonlinear optics.[52]

We have shown that both the optical and electronic properties of horizontally grown ZnO nanowires are quite similar to those of nonhorizontally grown ones. This indicates that the interaction with the substrate during growth does not induce defects that degrade the optical and electronic properties of the semiconductor, as opposed to epitaxial growth of 2D films. This important difference can be attributed to the fact that in a continuous film stress accumulates in two dimensions, whereas in a nanowire, stress only accumulates in the macroscopic axial direction but can be effectively released by contraction, expansion, or misfit dislocations in the transverse direction. Thus, guided VLS growth of horizontal nanowires enjoys the beneficial orientation control of epitaxial growth, without suffering the stress-related problems of traditional epitaxial growth in 2D layers. This new 1D nanoscale effect, together with the graphoepitaxial effect, constitutes a paradigm shift not only in the young field of nanowires but also in the long-established fields of epitaxy and thin films. This could pave the way to highly controlled semiconductor structures with potential applications not available by other means.

Last, we demonstrated the generality of the guided VLS approach for the growth of nanowires of different materials. This approach, demonstrated here for ZnO on sapphire and previously demonstrated for GaN, could be extended to a large variety of other semiconductors and other substrates, producing ordered arrays of nanowires and heterojunctions with coherently modulated composition and doping. This will enable the production of semiconductors with highly

controlled structures and unique properties, suitable for a wide range of applications, including nanocircuits, LEDs, lasers, photovoltaic cells, photodetectors, photonic and nonlinear optical devices.

METHODS

Substrate Preparation. Sapphire (α-Al_2O_3) wafers with eight different orientations were used. Singular (*i.e.*, well-cut) sapphire wafers, including C-plane (0001), M-plane ($10\bar{1}0$), A-plane ($11\bar{2}0$), and R-plane ($1\bar{1}02$), were purchased from Roditi International. Miscut C-plane (0001) sapphire wafers with different miscut directions were custom-produced as previously described. The manufacturer (Gavish Ltd., Omer, Israel) produced the wafers as directed, and the exact miscut tilt and azimuth angles were determined by our own developed procedure of asymmetric double exposure back-reflection XRD.[28] Miscut C-plane and M-plane sapphire substrates were annealed at 1100 and 1400 °C, respectively, in air, using a high-temperature muffle furnace (Carbolite RHF 16/8). Prior to use, the substrates were sonicated for 10 min in acetone, then rinsed in acetone, isopropyl alcohol (IPA), and distilled H_2O, and blow-dried in N_2.

Catalyst Deposition and Patterning. The Au catalyst was usually deposited by electron-beam evaporation of a thin (4−20 Å) metal layer. First, the areas for catalyst deposition were defined using standard photolithography with negative or positive photoresists. After pattern development and surface cleaning by oxygen plasma (March Plasmod GCM 200, 2 min, 1 sccm of O_2, 10 W) thin films (5−20 Å) of Au were deposited by electron-beam evaporation, followed by liftoff in acetone. These thin Au films undergo dewetting upon heating to 550 °C in air, thus generating the nanoparticles that serve as catalyst for the VLS growth of nanowires. In addition, deposition of Au catalyst nanoparticles was also performed by dispersing commercially available colloidal suspensions (British Biocell International), obtaining similar results.

Nanowire Synthesis. Nanowire growth was carried out in a quartz tube inside a tube furnace with fast heating capabilities (25 to 1000 °C in 5 min). The Zn and O atoms were supplied from ZnO powder mixed with carbon powder (1:1 mass ratio), held at 1000 °C, while the samples were held downstream at a temperature of 900 °C. N_2 was used as carrier gas (99.999%, Gordon Gas, further filtered to reduce O_2 and H_2O levels) at a flow of 500 sccm. In a typical experiment, a substrate with catalyst was placed on a fused silica carrier plate and inserted to a 25 mm diameter quartz tube. The tube was inserted into a split oven and purged of oxygen by 5 cycles of pumping to 3 mbar and purging with N_2 at elevated temperature. Once the tube was purged, N_2 was streamed into the tube, and pressure was maintained at 400 mbar. Once the desired temperature (1000 °C) is achieved, the oven was moved over the ZnO and graphite powder mixture and turned off at the end of the growth time (usually 5−30 min).

Microscopic Characterization. The grown nanowires were imaged using field-emission SEM (Supra 55VP FEG LEO Zeiss) at low working voltages (1−5 kV). Atomic force microscopy (AFM, Veeco, Multimode Nanoscope IV) images were acquired in air tapping mode. Thin lamellae for TEM characterization were made using a FEI Helios DualBeam microscope and inspected using a FEI Tecnai F30-UT field-emission TEM, equipped with a parallel EELS (Gatan imaging filter) operating at 300 kV. TEM digital images were recorded using a Gatan Ultrascan1000 CCD camera. TEM images were analyzed to determine crystallographic orientation and epitaxial relations using Fourier transform (FFT) from selected areas in the nanowire cross sections. Indexing of the FFT peaks was done according to crystallographic tables for bulk ZnO.

Optical Characterization. Photoluminescence spectra from single ZnO nanowires were acquired with a Jobin-Yvon LabRam HR 800 micro-Raman system, equipped with a liquid-N_2-cooled detector. For the excitation, we used a He−Cd laser at 325 nm. The laser power on the sample was 5 mW. The measurements were taken with a 2400 g mm^{-1} grating for the UV (spectral resolution 4 cm^{-1}) and a confocal microscope with a 100 μm aperture and a 10 μm laser spot.

Electrical Characterization. ZnO nanowire field-effect transistors (FETs) were fabricated by defining source and drain electrodes using electron-beam lithography (JEOL 6400 SEM equipped with JC Nabity Nanopattern Generator System), followed by electron-beam evaporation of Ti (20 nm)/Al(20 nm)/Pt-(20 nm)/Au (40 nm) to ensure low contact resistance,[53] and liftoff in acetone. For gate dielectric, 30 nm thick Al_2O_3 was deposited by atomic layer deposition (Fiji F200, Cambridge NanoTech). A top-gate electrode was patterned by electron-beam lithography, electron-beam evaporation (Ti 5 nm/Au 50 nm), and liftoff. The typical spacing between source and drain electrodes was 3 μm, with 1.5 μm wide gate electrode between.

Two-terminal electrical measurements were performed by applying source−drain DC bias and recording $I-V$ curves with different gate voltages. The charge carrier mobility μ was extracted from the transconductance g_m, which is defined as the slope of the $I_{sd}-V_g$ curve in the linear region and is given by eq 1, where V_g is the gate voltage, I_{dc} is the mobility, L is the nanowire channel length, and C is the capacitance.[54] The nanowire channel length L was defined by the gate electrode width, while the part of the nanowire uncovered by the gate electrode was considered as a parasitic resistor, with a constant resistance extracted from zero-field $I-V$ measurement. The capacitance is calculated using quasi-circular cross-section approximation given by eq 2, where h is the dielectric thickness and a is the width of the horizontal ZnO nanowire.[55] The carrier concentration n_e was extracted from the threshold voltage V_{th} using eq 3, where r is the nanowire radius and the total charge $Q = CV_{th}$.

$$g_m = \frac{dI_{dc}}{dV_g}\Big|_{V_{sd}=\text{const}} = \mu\left(\frac{C}{L^2}\right)V_{sd} \quad (1)$$

$$C \approx \frac{2\pi\varepsilon\varepsilon_0 L}{\ln(4h/a)} \quad (2)$$

$$Q = CV_{th} = n_e e\pi r^2 L \quad (3)$$

Conflict of Interest: The authors declare no competing financial interest.

Acknowledgment. We thank Dr. L. Zeiri for assistance with PL measurements. This research was supported by the Israel Science Foundation, Minerva Stiftung, Kimmel Center for Nanoscale Science, Moskowitz Center for Nano and Bio-Nano Imaging, and Djanogly, Alhadeff, and Perlman foundations. D.T. acknowledges support from the Adams Fellowship Program of the Israel Academy of Science.

Supporting Information Available: (1) Additional TEM images of guided ZnO nanowires on different substrates; (2) side-view TEM of a ZnO nanowire on M($10\bar{1}0$) sapphire; (3) ZnO growth on M-plane and R-plane sapphire with a statistically preferred growth direction; (4) TEM images of guided ZnO nanowires on different substrates with FFT insets of the nanowire and the substrate. This material is available free of charge *via* the Internet at http://pubs.acs.org.

REFERENCES AND NOTES

1. Lu, W.; Lieber, C. M. Nanoelectronics from the Bottom Up. *Nat. Mater.* **2007**, *6*, 841–850.
2. Cui, Y.; Lieber, C. M. Functional Nanoscale Electronic Devices Assembled Using Silicon Nanowire Building Blocks. *Science* **2001**, *291*, 851–853.
3. Huang, Y.; Duan, X. F.; Cui, Y.; Lauhon, L. J.; Kim, K. H.; Lieber, C. M. Logic Gates and Computation from Assembled Nanowire Building Blocks. *Science* **2001**, *294*, 1313–1317.

4. Duan, X. F.; Huang, Y.; Agarwal, R.; Lieber, C. M. Single-Nanowire Electrically Driven Lasers. *Nature* **2003**, *421*, 241–245.
5. Huang, M. H.; Mao, S.; Feick, H.; Yan, H. Q.; Wu, Y. Y.; Kind, H.; Weber, E.; Russo, R.; Yang, P. D. Room-Temperature Ultraviolet Nanowire Nanolasers. *Science* **2001**, *292*, 1897–1899.
6. Gudiksen, M. S.; Lauhon, L. J.; Wang, J.; Smith, D. C.; Lieber, C. M. Growth of Nanowire Superlattice Structures for Nanoscale Photonics and Electronics. *Nature* **2002**, *415*, 617–620.
7. Huang, Y.; Duan, X. F.; Cui, Y.; Lieber, C. M. Gallium Nitride Nanowire Nanodevices. *Nano Lett.* **2002**, *2*, 101–104.
8. Law, M.; Greene, L. E.; Johnson, J. C.; Saykally, R.; Yang, P. D. Nanowire Dye-Sensitized Solar Cells. *Nat. Mater.* **2005**, *4*, 455–459.
9. Tian, B.; Zheng, X.; Kempa, T. J.; Fang, Y.; Yu, N.; Yu, G.; Huang, J.; Lieber, C. M. Coaxial Silicon Nanowires as Solar Cells and Nanoelectronic Power Sources. *Nature* **2007**, *449*, 885–U8.
10. Yan, R. X.; Gargas, D.; Yang, P. D. Nanowire Photonics. *Nat. Photonics* **2009**, *3*, 569–576.
11. Cui, Y.; Wei, Q. Q.; Park, H. K.; Lieber, C. M. Nanowire Nanosensors for Highly Sensitive and Selective Detection of Biological and Chemical Species. *Science* **2001**, *293*, 1289–1292.
12. Kolmakov, A.; Zhang, Y. X.; Cheng, G. S.; Moskovits, M. Detection of CO and O_2 Using Tin Oxide Nanowire Sensors. *Adv. Mater.* **2003**, *15*, 997–1000.
13. Wan, Q.; Li, Q. H.; Chen, Y. J.; Wang, T. H.; He, X. L.; Li, J. P.; Lin, C. L. Fabrication and Ethanol Sensing Characteristics of ZnO Nanowire Gas Sensors. *Appl. Phys. Lett.* **2004**, *84*, 3654–3656.
14. Wang, Z. L.; Song, J. H. Piezoelectric Nanogenerators Based on Zinc Oxide Nanowire Arrays. *Science* **2006**, *312*, 242–246.
15. Huang, Y.; Duan, X. F.; Wei, Q. Q.; Lieber, C. M. Directed Assembly of One-Dimensional Nanostructures into Functional Networks. *Science* **2001**, *291*, 630–633.
16. Duan, X.; Niu, C.; Sahi, V.; Chen, J.; Parce, J. W.; Empedocles, S.; Goldman, J. L. High-Performance Thin-Film Transistors Using Semiconductor Nanowires and Nanoribbons. *Nature* **2003**, *425*, 274–278.
17. Smith, P. A.; Nordquist, C. D.; Jackson, T. N.; Mayer, T. S.; Martin, B. R.; Mbindyo, J.; Mallouk, T. E. Electric-Field Assisted Assembly and Alignment of Metallic Nanowires. *Appl. Phys. Lett.* **2000**, *77*, 1399–1401.
18. Liu, Y.; Chung, J.-H.; Liu, W. K.; Ruoff, R. S. Dielectrophoretic Assembly of Nanowires. *J. Phys. Chem. B* **2006**, *110*, 14098–14106.
19. Jin, S.; Whang, D. M.; McAlpine, M. C.; Friedman, R. S.; Wu, Y.; Lieber, C. M. Scalable Interconnection and Integration of Nanowire Devices without Registration. *Nano Lett.* **2004**, *4*, 915–919.
20. Whang, D.; Jin, S.; Wu, Y.; Lieber, C. M. Large-Scale Hierarchical Organization of Nanowire Arrays for Integrated Nanosystems. *Nano Lett.* **2003**, *3*, 1255–1259.
21. Tao, A. R.; Huang, J.; Yang, P. Langmuir–Blodgettry of Nanocrystals and Nanowires. *Acc. Chem. Res.* **2008**, *41*, 1662–1673.
22. Wang, D.; Chang, Y.-L.; Liu, Z.; Dai, H. Oxidation Resistant Germanium Nanowires: Bulk Synthesis, Long Chain Alkanethiol Functionalization, and Langmuir–Blodgett Assembly. *J. Am. Chem. Soc.* **2005**, *127*, 11871–11875.
23. Fan, Z. Y.; Ho, J. C.; Jacobson, Z. A.; Yerushalmi, R.; Alley, R. L.; Razavi, H.; Javey, A. Wafer-Scale Assembly of Highly Ordered Semiconductor Nanowire Arrays by Contact Printing. *Nano Lett.* **2008**, *8*, 20–25.
24. Takahashi, T.; Takei, K.; Ho, J. C.; Chueh, Y.-L.; Fan, Z.; Javey, A. Monolayer Resist for Patterned Contact Printing of Aligned Nanowire Arrays. *J. Am. Chem. Soc.* **2009**, *131*, 2102–2103.
25. Kuykendall, T.; Pauzauskie, P. J.; Zhang, Y. F.; Goldberger, J.; Sirbuly, D.; Denlinger, J.; Yang, P. D. Crystallographic Alignment of High-Density Gallium Nitride Nanowire Arrays. *Nat. Mater.* **2004**, *3*, 524–528.
26. Yang, C.; Zhong, Z. H.; Lieber, C. M. Encoding Electronic Properties by Synthesis of Axial Modulation-Doped Silicon Nanowires. *Science* **2005**, *310*, 1304–1307.
27. Ismach, A.; Kantorovich, D.; Joselevich, E. Carbon Nanotube Graphoepitaxy: Highly Oriented Growth by Faceted Nanosteps. *J. Am. Chem. Soc.* **2005**, *127*, 11554–11555.
28. Ismach, A.; Segev, L.; Wachtel, E.; Joselevich, E. Atomic-Step-Templated Formation of Single Wall Carbon Nanotube Patterns. *Angew. Chem., Int. Ed.* **2004**, *43*, 6140–6143.
29. Kocabas, C.; Hur, S.-H.; Gaur, A.; Meitl, M. A.; Shim, M.; Rogers, J. A. Guided Growth of Large-Scale, Horizontally Aligned Arrays of Single-Walled Carbon Nanotubes and Their Use in Thin-Film Transistors. *Small* **2005**, *1*, 1110–1116.
30. Nikoobakht, B.; Michaels, C. A.; Stranick, S. J.; Vaudin, M. D. Horizontal Growth and *In Situ* Assembly of Oriented Zinc Oxide Nanowires. *Appl. Phys. Lett.* **2004**, *85*, 3244–3246.
31. Nikoobakht, B.; Herzing, A. Formation of Planar Arrays of One-Dimensional p–n Heterojunctions Using Surface-Directed Growth of Nanowires and Nanowalls. *ACS Nano* **2010**, *4*, 5877–5886.
32. Fortuna, S. A.; Wen, J. G.; Chun, I. S.; Li, X. L. Planar GaAs Nanowires on GaAs (100) Substrates: Self-Aligned, Nearly Twin-Defect Free, and Transfer-Printable. *Nano Lett.* **2008**, *8*, 4421–4427.
33. Tsivion, D.; Schvartzman, M.; Popovitz-Biro, R.; von Huth, P.; Joselevich, E. Guided Growth of Millimeter-Long Horizontal Nanowires with Controlled Orientations. *Science* **2011**, *333*, 1003–1007.
34. Geis, M. W.; Flanders, D. C.; Smith, H. I. Crystallographic Orientation of Silicon on an Amorpous Substrate Using an Artificial Surface-Relief Grating and Laser Crystallization. *Appl. Phys. Lett.* **1979**, *35*, 71–74.
35. Choi, J. H.; Kim, D. Y.; Hockey, B. J.; Wiederhorn, S. M.; Handwerker, C. A.; Blendell, J. E.; Carter, W. C.; Roosen, A. R. Equilibrium Shape of Internal Cavities in Sapphire. *J. Am. Ceram. Soc.* **1997**, *80*, 62–68.
36. Morkoç, H.; Özgür, U., *Zinc Oxide: Fundamentals, Materials and Device Technology*; Wiley-VCH: Weinheim, Germany, 2009.
37. Nikoobakht, B.; Eustis, S.; Herzing, A. Strain-Driven Growth of Zinc Oxide Nanowires on Sapphire: Transition from Horizontal to Standing Growth. *J. Phys. Chem. C* **2009**, *113*, 7031–7037.
38. Gabai, R.; Ismach, A.; Joselevich, E. Nanofacet Lithography: A New Bottom-Up Approach to Nanopatterning and Nanofabrication by Soft Replication of Spontaneously Faceted Crystal Surfaces. *Adv. Mater.* **2007**, *19*, 1325–1330.
39. Shi, J.; Sun, X.; Zhang, J.; Lian, J.; Yu, Q.; Lin, M.; Li, H. Epitaxial Growth of Horizontally Aligned Zinc Oxide Nanonecklace Arrays on R-Plane Sapphire. *J. Phys. Chem. C* **2009**, *113*, 20845–20854.
40. Schmidt, V.; Senz, S.; Gösele, U. Diameter-Dependent Growth Direction of Epitaxial Silicon Nanowires. *Nano Lett.* **2005**, *5*, 931–935.
41. Fu, Z.; Wang, Z.; Yang, B.; Yang, Y.; Yan, H.; Xia, L. Shape-Control of Nano-ZnO by Changing the Solvent. *Mater. Lett.* **2007**, *61*, 4832–4835.
42. Kong, X. Y.; Wang, Z. L. Spontaneous Polarization-Induced Nanohelixes, Nanosprings, and Nanorings of Piezoelectric Nanobelts. *Nano Lett.* **2003**, *3*, 1625–1631.
43. Kurtz, M.; Strunk, J.; Hinrichsen, O.; Muhler, M.; Fink, K.; Meyer, B.; Wöll, C. Active Sites on Oxide Surfaces: ZnO-Catalyzed Synthesis of Methanol from CO and H_2. *Angew. Chem., Int. Ed.* **2005**, *44*, 2790–2794.
44. Kong, Y. C.; Yu, D. P.; Zhang, B.; Fang, W.; Feng, S. Q. Ultraviolet-Emitting ZnO Nanowires Synthesized by a Physical Vapor Deposition Approach. *Appl. Phys. Lett.* **2001**, *78*, 407–409.
45. Lin, B. X.; Fu, Z. X.; Jia, Y. B. Green Luminescent Center in Undoped Zinc Oxide Films Deposited on Silicon Substrates. *Appl. Phys. Lett.* **2001**, *79*, 943–945.
46. Vanheusden, K.; Warren, W. L.; Seager, C. H.; Tallant, D. R.; Voigt, J. A.; Gnade, B. E. Mechanisms Behind Green Photoluminescence in ZnO Phosphor Powders. *J. Appl. Phys.* **1996**, *79*, 7983–7990.

47. Ghosh, R.; Basak, D.; Fujihara, S. Effect of Substrate-Induced Strain on the Structural, Electrical, and Optical Properties of Polycrystalline ZnO Thin Films. *J. Appl. Phys.* **2004**, *96*, 2689–2692.
48. Goldberger, J.; Sirbuly, D. J.; Law, M.; Yang, P. ZnO Nanowire Transistors. *J. Phys. Chem. B* **2004**, *109*, 9–14.
49. Beaumont, B.; Vennéguès, P.; Gibart, P. Epitaxial Lateral Overgrowth of GaN. *Phys. Status Solidi B* **2001**, *227*, 1–43.
50. Schwarz, K. W.; Tersoff, J. Elementary Processes in Nanowire Growth. *Nano Lett.* **2011**, *11*, 316–320.
51. Wood, C.; Jena, D. *Polarization Effects in Semiconductors: From Ab Initio Theory to Device Applications*; Springer: Berlin, 2008.
52. Okumura, H.; Shimizu, M.; Qiang Shen, X.; Ide, T. Polarity Control in MBE Growth of III-Nitrides, and Its Device Application. *Curr. Appl. Phys.* **2002**, *2*, 305–310.
53. Ip, K.; Baik, K. H.; Heo, Y. W.; Norton, D. P.; Pearton, S. J.; LaRoche, J. R.; Luo, B.; Ren, F.; Zavada, J. M. Annealing Temperature Dependence of Contact Resistance and Stablity for Ti/Al/Pt/Au Ohmic Contacts to Bulk n-ZnO. *J. Vac. Sci. Technol., B* **2003**, *21*, 2378–2381.
54. Martel, R.; Schmidt, T.; Shea, H. R.; Hertel, T.; Avouris, P. Single- and Multi-Wall Carbon Nanotube Field-Effect Transistors. *Appl. Phys. Lett.* **1998**, *73*, 2447–2449.
55. Cui, Y.; Duan, X.; Hu, J.; Lieber, C. M. Doping and Electrical Transport in Silicon Nanowires. *J. Phys. Chem. B* **2000**, *104*, 5213–5216.
56. Iwanaga, H.; Kunishige, A.; Takeuchi, S. Anisotropic Thermal Expansion in Wurtzite-Type Crystals. *J. Mater. Sci.* **2000**, *35*, 2451–2454.
57. Kondo, S.; Tateishi, K.; Ishizawa, N. Structural Evolution of Corundum at High Temperatures. *Jpn. J. Appl. Phys.* **2008**, *47*, 616.